Appl Water Sci (2013) 3:1–11
DOI 10.1007/s13201-013-0079-0

REVIEW ARTICLE

Identification of raining clouds using a method based on optical and microphysical cloud properties from Meteosat second generation daytime and nighttime data

Mourad Lazri · Soltane Ameur · Jean Michel Brucker · Jacques Testud · Bachir Hamadache · Slimane Hameg · Fethi Ouallouche · Yacine Mohia

Received: 27 August 2012 / Accepted: 2 January 2013 / Published online: 30 January 2013

Abstract A new scheme for the delineation of raining and non-raining cloud areas applicable to mid-latitudes from daytime and nighttime multispectral satellite data is developed. The technique is based on optical and microphysical cloud properties using an artificial neural network. The tests have been conducted during the rainy season of 2006/2007. The proposed algorithm uses the spectral parameters of SEVIRI (Spinning Enhanced Visible and Infrared): brightness temperature $T_{IR10.8}$ and brightness temperature differences $\Delta T_{IR10.8–IR12.1}$, $\Delta T_{IR8.7–IR10.8}$, $\Delta T_{IR3.9–IR10.8}$ and $\Delta T_{IR3.9–WV7.3}$ during the nighttime and reflectances $R_{VIS0.6}$, $R_{NIR1.6}$, brightness temperature $T_{IR10.8}$, brightness temperature difference $\Delta T_{IR8.7–IR10.8}$ and $\Delta T_{IR10.8–IR12.0}$ during the daytime. The algorithm is calibrated by instantaneous meteorological radar using multilayer perceptron. Radar provided the ''ground precipitation truth'' for training and validation. The application shows interesting and encouraging results.

Keywords Meteorological satellite · Mediterranean climate · Properties of clouds, convective and stratiform clouds

M. Lazri (✉) · S. Ameur · S. Hameg · F. Ouallouche · Y. Mohia
Laboratoire LAMPA, University of Tizi Ouzou, Tizi Ouzou, Algeria
e-mail: m_lazri@yahoo.fr

S. Ameur
e-mail: ameursoltane@yahoo.com

S. Hameg
e-mail: hamegslimane@hotmail.fr

F. Ouallouche
e-mail: ouafethi_04@yahoo.fr

Y. Mohia
e-mail: mohiayacine@yahoo.fr

J. M. Brucker
School EPMI, EPMI—13 Boulevard de l'Hautil, 95092 Cergy Pontoise Cedex, Paris, France
e-mail: jm.brucker@epmi.fr

J. Testud
Novimet, 11 boulevard d'Alembert, 78280 Guyancourt, Paris, France
e-mail: jacques.testud@novimet.com

B. Hamadache
Office National de Météorologie, ONM (Algeria), Algiers, Algeria
e-mail: b.hamadache@meteo.dz

Introduction

Remote sensing data are now widely used for different purposes, and the use of satellite data for rainfall estimates has increased recently. Meteorological satellites are the only instruments capable to provide large amounts of rainfall measurements in remote areas where data are difficult or impossible to collect from the ground. For this purpose, rainfall estimates using meteorological satellite data [e.g. Meteosat Second Generation (MSG), National Oceanic and Atmospheric Administration (NOAA), Tropical Rainfall Measuring Mission (TRMM), TERRA, etc.] started since their commissioning. Several research works have been published in the literature (e.g. Stephens and Kummerow 2007; Levizzani et al. 2001; Levizzani 2003; Nauss and Kokhanovsky 2006). Programs such as Global Precipitation Climate Project (GPCP) (Ebert et al. 1996), Climate Prediction Center using Goes Precipitation Index (CPC) (Herman et al. 1997), Estimation of Precipitation using Satellite (EPSAT) (Berges et al. 2010;

Jobard et al. 2011), Tropical Applications in Meteorology using Satellite data (TAMSAT) (e.g. Grimes et al. 1999), Global Atmosphere Research Programme (GARP) (Arkin 1979) have also been developed and applied to rainfall estimates. Techniques researching the relationship between thermal infrared and intensity of precipitation have been widely used (e.g. Mishra et al. 2011; Adler and Negri 1988; Tarruella and Jorge 2003) or Cold Cloud Durations (CCD) (e.g. Huffman et al. 2001; Grimes et al. 1999; Arkin 1979).

According to the precipitation processes in connection with extratropical cyclones, convectively dominated precipitation areas are characterized by a large vertical extension and a cloud top rising high into the atmosphere. As a result, the established relationship between cloud-top temperature (CTT) and rainfall probability and intensity can be applied for the detection and classification of these precipitation areas. However, it becomes also visible that the advective-stratiform precipitation areas, that form a major part of the precipitating cloud areas in connection with extra-tropical cyclones, are not necessarily connected to cold CTT. As a consequence, a CTT threshold does not seem to be effective for the detection and classification of these areas.

For that reason, some authors have suggested to use optical and microphysical cloud proprieties to identify the raining clouds even in stratiform systems from TRMM satellite (e.g. Lensky and Rosenfeld 2003a, b) or from Terra-MODIS satellite (e.g. Nauss and Kokhanovsky 2006; Platnick et al. 2003). These techniques are based on the use of information about droplet diameter, optical thickness and thermodynamical phase of clouds. A raining cloud requires a high optical thickness, a large effective particle radius and the presence of ice crystals in the top.

The arrival of MSG gave a breakthrough for the classification of clouds. The SEVIRI radiometer (Spinning Enhanced Visible and Infrared) on board MSG provides more condensed information and its frequency of observation changes from 30 to 15 min. Multispectral capacity increases to 12 channels. The spatial resolution changes from 2.5 to 1 km at nadir for broadband visible channel and 5–3 km for all other channels.

The simultaneous use of its spectral parameters provides information about microphysical and optical cloud properties. Several techniques have been therefore developed to identify the raining clouds from multispectral parameters of SEVIRI radiometer (e.g. Kobayashi 2007; Roebeling and Holleman 2009; Wolters et al. 2011; Nauss and Kokhanovsky 2006; Thies et al. 2008a, b). These approaches are not only applicable to the detection of mainly convective precipitation by means of the commonly used relation between infrared cloud-top temperature and rainfall probability but enables also the detection of stratiform precipitation (e.g. in connection with mid-latitude frontal systems).

Therefore, the objective of the present paper is to propose a new operational technique for rain area delineation in the mid-latitudes on a 15-min basis for MSG/SEVIRI daytime and nighttime data. It is applied to the complex situation of the Mediterranean climate of this region and takes into account the variation of the diurnal cycle of clouds. The technique is based on information about optical and microphysical cloud properties from MSG/SEVIRI. It is calibrated by instantaneous meteorological radar data using multilayers perceptron. Artificial neural networks (NNs), widely used in precipitation remote sensing (Bellerby et al. 2000; Grimes et al. 2003; Tapiador et al. 2004), are the statistical tool chosen to define the correlations between satellite measurements and classes of ground precipitation as estimated by weather radars.

Presentation of study region and datasets

Algeria is located on the South shore of the Mediterranean region; it is bordered on the East by Tunisia and Libya, on the South by Niger and Mali, South-West by Mauritania and Western Sahara and West by Morocco. This region has a particular orographic structure and special characteristics of the sea-land coast. Due to these geographical properties, its climate has a very complex spatio-temporelle feature (Lionello et al. 2006). Indeed, it is influenced by both the subtropical climate and the climate of mid-latitude systems (Trigo et al. 2006; Alpert et al. 2006). The spatial distribution of precipitation is characterized by a very marked North–South gradient and a very low East–West gradient. The rainy season extends from October to March, with maximum rainfall occurring during November–December. In the north, the climate is Mediterranean transit, marked by seasonal oscillations. The average annual rainfall is estimated at about 600 mm. The minimum rainfall is recorded in the southern regions. It is about 50 mm while the maximum is observed in the Djurdjura massif located in Kabylia and the massif of Edough located a little farther east, where it exceeds 1,500 mm. The study area in this work is located in the north of Algeria, on domain with a radius of 250 km (Fig. 1). In Fig. 1, the red circle shows the domain of radar which coincides with the study area.

For this study, MSG/SEVIRI data together with corresponding ground-based radar data are required.

MSG/SEVIRI data

The dataset used in this work provided by the SEVIRI radiometer of Meteosat-8 in different frequency bands is collected from November 2006 to March 2007 and November 2009 to March 2010. The MSG is a spinning stabilized satellite that is positioned at an altitude of about

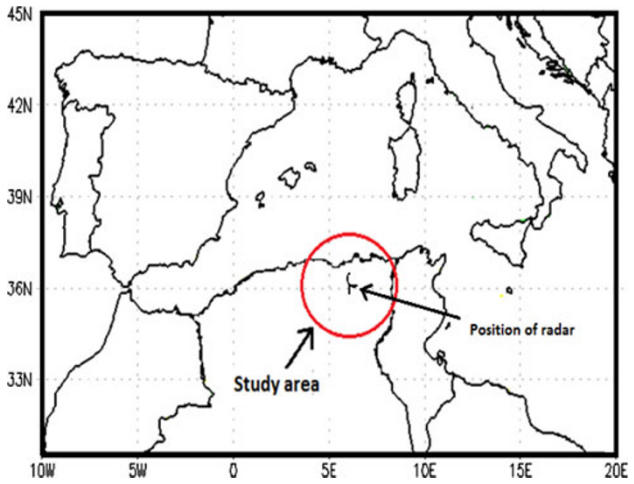

Fig. 1 The study area and the position of the weather radar of Setif. The *red circle* shows the radar domain with a radius of 250 km

36,000 km above the equator at 3.4°W. The SEVIRI radiometer gives every 15 min 12 images in the 12 available channels. We selected the channels sensitive to optical and microphysical properties of clouds (optical thickness, droplet size, cloud phase) as well as to the temperature of cloud tops, and those located in the spectral absorption bands mainly affected by the water vapor. These channels correspond to bands: visible (VIS0.6), near infrared (NIR1.6), water vapor (WV6.2, WV7.3) and infrared (IR3.9, IR8.7, IR10.8 and IR12.0). The raw image (level 1.5) has a size of 3,712 × 3,712 pixels in each channel (Eumetsat 2004). This corresponds to a spatial resolution at the image center of about 3 km. Each pixel is coded on 10 bits. All pixels are geolocalized on a common grid in geostationary projection. The sub-satellite point corresponds to the pixel position (1,856, 1,856) on the image. We stored the raw data (level 1.5), i.e. the values of 3,712 × 3,712 pixels of the image, and the calibration coefficients to deduce the radiance for each pixel. For our case, we have predefined an area in the image of the Earth's surface; it corresponds to our study region (Fig. 1).

Meteorological radar data

The radar data are provided by the ground-based C band radar network of The National Office of Meteorology (ONM). The radar of Setif is installed near to the town of Setif, at 36°11′N, 5°25′E and 1,700 m of altitude, is one of seven Algerian meteorological radars. This is a Radar AWSR 81C in Cband, its operational frequency is 5.6 GHz. The displacement in azimuth is between 0° and 360° in continuous and the movement in inclination is of −1° to 90°. Its polarization is linear and horizontal. The effective domain of radar is a radius of 250 km.

Meteorological radar data are collected at a temporal resolution of 15 min and a spatial resolution of 1 km in a format of 512 × 512 pixels. Each pixel is coded on four bits. Thus, it consist of 15 classes representing different reflectivity intensities which are all together considered as raining in the comparison with collocated satellite pixels and one class representing no raining. The physical parameter of the radar is the reflectivity factor, referred to as Z and expressed in (mm^6/m^3). The conversion of reflectivity factor Z into rainfall intensity R (mm/h) is obtained using the Eq. (1) adapted to our Radar and can also be converted into dBZ:

$$Z = 300\,R^{1.5} \tag{1}$$

The scan interval for both data sets is 15 min. For the spatial comparison the radar data with an original spatial resolution of 1 × 1 km were projected to the viewing geometry of SEVIRI with a spatial resolution of 4 × 5 km in the study area.

Because of discrepancies between the SEVIRI data and radar data, due to differences in observation time, parallax errors and collocation errors (Vicente et al. 2002), the comparison of these types of data may be hampered. To reduce the imbalances mentioned above and find a better correlation, we performed a repositioning to SEVIRI data to coincide spatially with radar data. We also applied a resampling to radar data to have the same resolution as resolution of satellite data. The resolution is 4 × 5 km in the study region and is assumed constant due to low overlapped area observed by both sensors. Therefore, each SEVIRI pixel is collocated with 4 × 5 radar pixels. The time lag between the radar and the satellite is about 3 min. This small time difference does not require synchronization between the two data types.

Methodology

Both datasets (SEVIRI and Radar) are divided into a training and validation data set. The training data set used for the development of the technique is collected from November 2006 to March 2007. The validation data set considered for the appraisal of the proposed technique is recorded between November 2009 and March 2010.

Because of the differing information about optical and microphysical cloud properties between day-time and night-time scenes, both data sets are divided into day- and night-time scenes.

We have hence created two identical neural networks for identifying of rainfall. The first one is used during the daytime and the second one is applied during nighttime (see Fig. 5). Each neural network used in this scheme is a multilayer perceptron (Rosenblatt 1962). The target outputs

of the neural network correspond to radar data. A neural network learns the input–output relationship through the training process. The learning process in a neural network is an interactive procedure in which its connection weights are adapted through the presentation of a set of input–output training example pairs.

The neural network algorithm

The kind of neural network used for this study is a feed-forward multiple-layer perceptron (MLP). The MLP has a relatively simple architecture in which each node receives output only from nodes in the preceding layer and provides input only to nodes in the subsequent layer. Thus, for the node j in the kth layer the net input l_{kj} is a weighted average of the outputs of the $(k-1)$th layer :

$$l_{kj} = \sum_{i=1}^{N_{k-1}} w_{(k-1)ij}\, O_{(k-1)i} \tag{2}$$

where $w(k-1)_{ij}$ is the weight connecting the output of the node i in the $(k-1)$th layer to node j in the kth layer and N_{k-1} is the number of nodes in the $(k-1)$th layer. The output of node j is a specified function of l_{kj}:

$$O_{kj} = f(l_{kj}) \tag{3}$$

The eventual output is then a function of the weighted combination of the final hidden-layer output values.

The list of inputs is information extracted from SEVIRI. The full list is shown in Fig. 5a during daytime and in Fig. 5b during nighttime. Each architecture is consisted of four layers: input, output, and two hidden layers. The transfer function relating input to output was a sigmoid function:

$$O_{kj} = \left[1 + \exp(-2l_{kj})\right]^{-1} \tag{4}$$

To ensure that the model has similar sensitivity to changes in the various inputs, all of the inputs were normalized to values between 0 and 1. For an input variable x with maximum $x_{\max}$ and minimum $x_{\min}$ we calculate the normalized value x_A as:

$$x_A = \frac{x - x_{\min}}{x_{\max} - x_{\min}} \tag{5}$$

The optimum weights were determined by training against the target values. The Fig. 2 shows the structure of a neuron with the transfer function relating input to output.

Three-layer perceptron network for function approximation

The rainfall estimation problem can be viewed as a complex function approximation problem. The universal approximation theorem for neural network states that a two-layer feed forward perceptron network with nonconstant, bounded, and monotone-increasing continuous activation function can perform arbitrary nonlinear input–output relationship mapping (Haykin 1994). Therefore, a two-layer perceptron network can be used for the rainfall estimation problem. The above universal approximation theorem gives the theoretical justification for the approximation of an arbitrary continuous function by a two-layer (one hidden-layer) perceptron network. In practice, however, a three-layer (two hidden-layer) perceptron network works better than a two layer perceptron for the function approximation problem. This is because the interaction between neurons in a single hidden layer network makes it difficult to obtain a globally good approximation, while a two-hidden layer network isolates and thus reduces the interaction effects by solving the problem in two steps, i.e. the first hidden-layer extracts the local features of the input data whereas the second hidden-layer extracts the global feature, to make the approximations in different regions of the input space individually adjusted (Haykin 1994). Due to above reasons, multilayer perceptron networks have been chosen in this paper for the rainfall identification problem. The structure of this multilayer perceptron with two hidden layers is shown in Fig. 5.

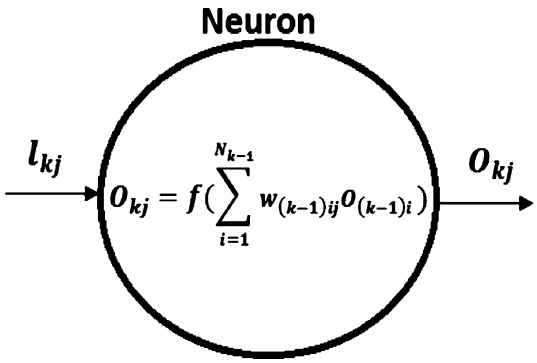

Fig. 2 Structure of a neuron of MLP

Training and testing data generation

A representative training data set consisting of the SEVIRI data and corresponding Radar data are needed to develop a multilayer perceptron for the rainfall identification problem. SEVIRI data are applied to the network as the input and the corresponding Radar data are used as the target or desired output (Fig. 5). The training procedure for a multilayer perceptron includes two steps, namely forward propagation and backward propagation.

The connectional weights are updated during the backward error propagation according to the learning algorithm. This process is repeated until the error between the network output and desired output (radar measurements) meets the prescribed requirement. When the training process is

complete, the network is ready for application. Rainfall identification can be obtained if SEVIRI data are applied to the network at this stage.

Application

The neural network MLP was created using five spectral parameters that were calculated from SEVIRI radiometer to discriminate raining cloud from no raining cloud. It was created with four layers (input, two hidden, and output) that consist of five input neurons, six neurons in the first hidden layer, five neurons in the second hidden layer and two output neurons in the output layer that represent the two classes (raining and no raining) corresponding to radar data (Fig. 5). The information about optical and microphysical cloud properties derived from SEVIRI used as input data to Artificial neural networks MLP are given as follows:

Information about "Cloud Water Path (CWP)" The effective droplet radius r_e and the optical thickness τ of clouds both represented by a single parameter referred to as CWP are directly related to rainfall probability of a cloud. The effective particle radius (r_e) defined by the ratio between the third and the second power of the droplet spectrum is taken in place of the actual droplet spectrum. The cloud optical thickness (τ) defined by the integration of the extinction coefficient integrated over the cloud geometrical thickness is considered representatively for the cloud geometrical thickness. The CWP represents the amount of water vertically integrated in the cloud and depends on the diameter of raindrops and the thickness of the cloud formed by these drops. The relationship is given by the following equation (Thies et al. 2008a, b; Nauss and Kokhanovsky 2006):

$$\mathrm{CWP} = \frac{2}{3}\,\rho\,\tau\,r_e \qquad (6)$$

where ρ (g/m^3) is the density of water in the clouds.

The CWP is related to the rainfall probability of a cloud and can therefore be used as a delimiter between the non-raining and raining cloud (e.g. Thies et al. 2008a, b; Nauss and Kokhanovsky 2006).

Information about "thermodynamic phase of cloud" To strengthen the above probability, some authors hypothesize that a cloud is more likely to produce rainfall for frontal processes if the water droplets and ice crystals coexist (phase of the cloud) (Thies et al. 2008a, b; Roebeling et al. 2007; Feidas and Giannakos 2010, 2011; Levizzani et al. 2001; Levizzani 2003). Indeed, the frontal systems are mainly associated with particles of ice in the upper clouds according to the Bergeron–Findeisen process (Houze 1993). Therefore, the intensity of precipitation in clouds is related to thermodynamic phase of cloud and CWP. This means that precipitating clouds are characterized by a large enough CWP and the existence of ice particles in the upper part of the cloud.

The technique we present for the identification of precipitating clouds is based on these assumptions. It is a technique based on optical and microphysical cloud properties that was originally developed and applied to SSM/I data (Special Sensor Microwave/Imager) (Wentz and Spencer 1998). We will apply it to the radiances measured in different bands of SEVIRI. Reflectances and brightness temperatures are used during the daytime (in the presence of solar radiation) and only brightness temperatures are used during the nighttime.

Identification of the precipitating cloud during daytime

The CWP (i.e. values of r_e and τ) considered for a rainfall intensity differentiation can be retrieved on a pixel basis during daytime using a combination of two solar channels (i.e. a VIS and a NIR channel). Radiances obtained in the band (0.4 and 0.8 μm) are usually used to estimate the optical thickness of clouds (Arking and Childs 1985). While the band between (1.6 and 3.9 μm) is a function that depends on effective droplet radius of cloud (Baum et al. 2000; Arking and Childs 1985). The combination of these two bands can provide useful information about optical thickness and effective droplet radius of cloud. Indeed, the information about the CWP can be derived implicitly using both reflectance $R_{\mathrm{VIS0.6}}$ of visible channel (VIS0.6) and reflectance $R_{\mathrm{NIR1.6}}$ of near-infrared channel (NIR1.6) from SEVIRI (e.g. Thies et al. 2008a; Roebeling et al. 2007; Roebeling and Holleman 2009). High values of $R_{\mathrm{VIS0.6}}$ correspond to high optical depth of cloud and low values of $R_{\mathrm{NIR1.6}}$ indicate large particles in the cloud. This means that a large CWP is obtained when high values of VIS0.6 coincide with low values of NIR1.6. However, because no operational retrieval technique is currently available for MSG SEVIRI, that is applicable to water and ice clouds, and that is fast enough concerning the 15-min scan cycle, the authors decided to use the original reflectance of cannel (VIS0.6) and cannel (NIR1.6) SEVIRI channels, instead of computed values of effective droplet radius and optical thickness of clouds. The Fig. 3 shows CWP as a function of $R_{\mathrm{VIS0.6}}$ versus $R_{\mathrm{NIR1.63}}$.

To determine the cloud phase (CP), which is also an important parameter for the identification of precipitating clouds; some authors have used information obtained from the difference of brightness temperature $\Delta T_{\mathrm{IR8.7–IR10.8}}$ (e.g. Strabala et al. 1994; Thies et al. 2008b). Others have defined a threshold of brightness temperature in the band IR10.8 to discriminate between cloud ice and cloud water (Rossow and Schiffer 1999). While Wolters et al. (2008) showed that the simultaneous use of $T_{\mathrm{IR10.8}}$ and $\Delta T_{\mathrm{IR8.7–IR10.8}}$ gives more accurate identification of the thermodynamic phases of

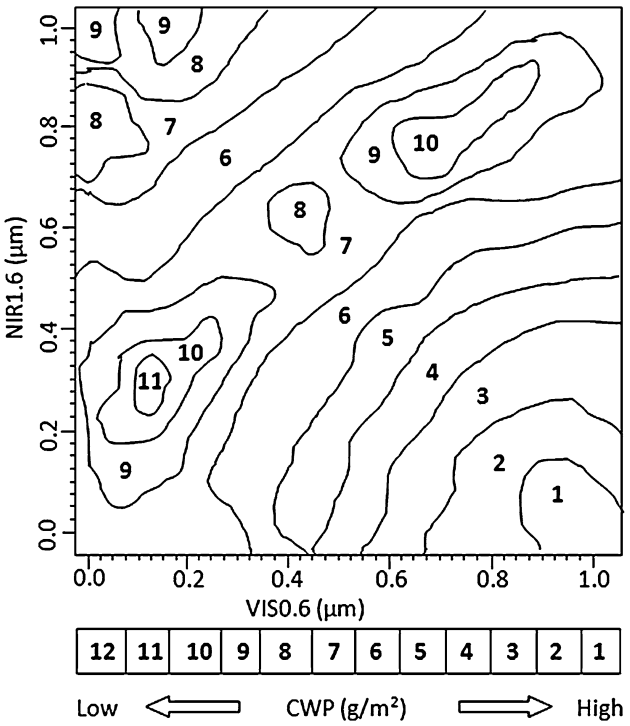

Fig. 3 Cloud water path as a function of $R_{VIS0.6}$ versus $R_{NIR1.63}$

clouds. They found that the formation of ice crystals begin when $T_{IR10.8} < 238$ K and $\Delta T_{IR8.7–IR10.8} > 0.25$ K. It should be noted that a cloud is likely to produce precipitation when ice crystals are present at the top of cloud.

Besides, the brightness temperature difference $\Delta T_{IR10.8–IR12.1}$, which is a good indicator of the cloud optical thickness, is very useful to discriminate optically thick cumuliform clouds from optically thin cirrus clouds (Feidas 2011; Inoue 1985, 1987a). Optically thick cumulus-type cloud shows the smaller $\Delta T_{IR10.8–IR12.1}$ due to their black-body characteristics, while optically thin cirrus cloud shows the larger $\Delta T_{IR10.8–IR12.1}$ due to the differential absorption characteristics of ice crystals between the two channels (Inoue et al. 2001). It is expected that optically thick and deep convective clouds are associated with rain (Inoue 1987b). Even though the split window technique is very effective in detecting and removing optically thin cirrus clouds with no precipitation, it sometimes incorrectly assigns optically thick clouds like cumulonimbus in place of optically thin clouds (Inoue 1997).

Five parameters were therefore chosen to identify raining clouds during the daytime (Fig. 5a): $R_{VIS0.6}$, $R_{NIR1.6}$, $T_{IR10.8}$, $\Delta T_{IR10.8–IR12.1}$ and $\Delta T_{IR8.7–IR10.8}$. This is carried out during solar illumination over the study area. To avoid errors due to low solar radiation, we used the radiances only when the zenith angle of the sun is between 0° and 70° relative to the study area.

Identification of precipitating clouds during nighttime

The night-time technique is based on the same conceptual model as the presented daytime scheme. However, since no operational retrieval exists for MSG to compute the CWP during nighttime, suitable combinations of brightness temperature $T_{IR10.8}$ and brightness temperature differences $\Delta T_{IR10.8–IR12.1}$, $\Delta T_{IR8.7–IR10.8}$, $\Delta T_{IR3.9–IR10.8}$ and $\Delta T_{IR3.9–WV7.3}$ are used to infer implicit information about microphysical and optical cloud properties.

The combination of the channel IR3.7 with the channel IR11 was already used to extract information about microphysical and optical cloud properties (e.g. Hutchison et al. 2006; Lensky and Rosenfeld 2003a).

Lensky and Rosenfeld (2003a, b) attempted to relate the brightness temperature difference $\Delta T_{IR3.7–IR11}$ of satellite TRMM to effective particle radius and to cloud optical thickness. They showed that for a cloud-top temperature higher than 260 K, precipitation is obtained when the $\Delta T_{IR3.7–IR11}$ is in the interval]1 K, 4 K[. Values lower than the interval are obtained when the cloud is optically thick with small effective particle radius. Values higher than the interval correspond to a semi-transparent cloud. These two situations correspond to a non-raining cloud. Thies et al. (2008b) used the channel IR3.9 and the channel IR10.8 of SEVIRI radiometer on ice clouds and water clouds. They get the same conclusions as Lensky and Rosenfeld (2003a, b). Indeed, a precipitating cloud indicates mean values for $\Delta T_{IR3.9–IR10.8}$.

In general, $\Delta T_{IR3.9–WV7.3}$ should show similar characteristics as $\Delta T_{IR3.9–IR10.8}$. Because of the diminishing effect of the water vapor absorption and emission in mid- to low-tropospheric levels on the brightness temperature (BT) in the channel (WV7.3) (Schmetz et al. 2002), $\Delta T_{IR3.9–WV7.3}$ should be generally higher than $\Delta T_{IR3.9–IR10.8}$. Therefore, $\Delta T_{IR3.9–WV7.3}$ is expected to provide additional information about the CWP. For thin clouds with small or large particles, respectively (small or medium CWP), $T_{IR3.9}$ is larger than $T_{WV7.3}$ and $\Delta T_{IR3.9–WV7.3}$ reaches the highest values. Large particles together with a high optical thickness (high CWP) result in medium to high difference values, which are lower than for optically thin clouds. Thick clouds with small particles (medium CWP) lead to small $\Delta T_{IR3.9–WV7.3}$.

Therefore, we use suitable combinations of brightness temperature differences (ΔT) between the thermal bands of MSG SEVIRI to infer qualitative information on CWP ($\Delta T_{IR3.9–WV7.3}$ and $\Delta T_{IR3.9–IR10.8}$) (Thies et al. 2008b; Feidas and Giannakos 2011). The CWP as a function of $\Delta T_{IR3.9–IR10.8}$ versus $\Delta T_{IR3.9–WV7.3}$ is given in the Fig. 4.

In addition, $\Delta T_{IR8.7–IR10.8}$ and $\Delta T_{IR10.8–IR12.0}$ are particularly considered to supply information about the cloud phase. Similar to the daytime approach, rain area delineation is realized by means of the pixel-based rainfall

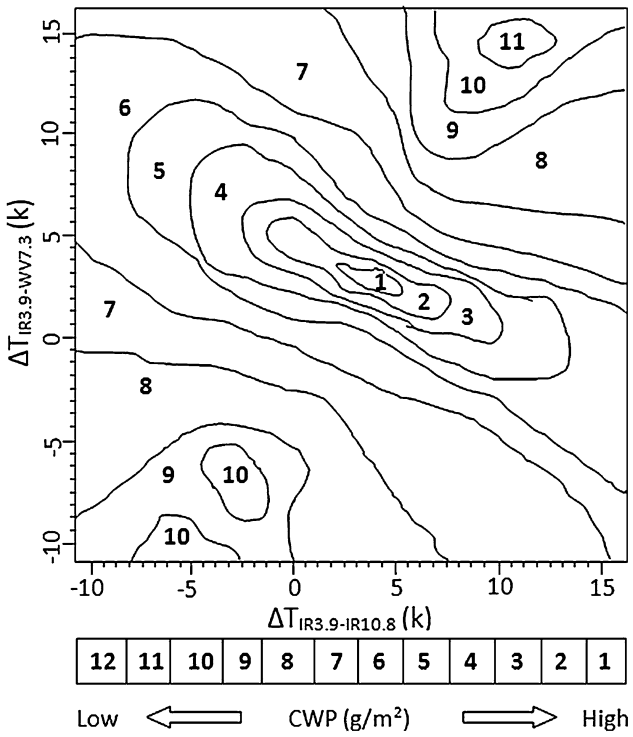

Fig. 4 Cloud water path as a function of $\Delta T_{IR3.9–IR10.8}$ versus $\Delta T_{IR3.9–WV7.3}$

confidence as a function of the respective value combination of the brightness temperature differences. To these parameters, we add $T_{IR10.8}$, $\Delta T_{IR10.8–IR12.0}$ and $\Delta T_{IR8.7–IR10.8}$ to identify precipitating clouds as mentioned previously for daytime.

In summary, we have decided to use parameters $\Delta T_{IR3.9–IR10.8}$ and $\Delta T_{IR10.8–IR12.0}$ that provide information about the CWP, and we incorporate the $\Delta T_{IR8.7–IR10.8}$, $\Delta T_{IR10.8–IR12.0}$ and $T_{IR10.8}$, which give information about the thermodynamic phase and thickness of cloud.

The parameters presented previously will be used as input data, and information about rain from meteorological radar as output data (Fig. 5). The MPL rain delineation algorithms during daytime were trained using five spectral parameters (Fig. 5a) and the MPL during nighttime were trained using five spectral parameters (Fig. 5b). These parameters were computed from SEVIRI dataset during the period November 2006 to March 2007.

Rainfall identification results and performance evaluation

Models are validated against independent rainy days during November 2009 to March 2010, not used for training the rain area delineation algorithms. The evaluation was performed by comparison with instantaneous ground-based radar data collocated with SEVIRI data. The aim is to evaluate the potential of MLP algorithm in the identification of precipitation. The observation scenes made by the radar and satellite at a rhythm of 15 min are 15,880, most of which are non-raining situations.

To evaluate the potential improvement by the new scheme, the validation scenes were also classified by the Enhanced Convective Stratiform Technique (ECST) (Reudenbach et al. 2001) which is similar to the Convective Stratiform Technique (CST) (Adler and Negri 1988). The method CST originally developed by Adler and Negri (1988) uses a temperature threshold to identify convective cores. Adjacent pixels are identified as stratiform according to their levels of temperature and the area occupied by these pixels. This technique was applied successfully in tropical convective systems (Bendix 1997). However, it shows limits in the extratropical region (Negri and Adler 1993). Reudenbach et al. (2001) adjusted the technique CST to be applied to convective systems in the mid-latitude. The ECST additionally includes the water vapor channel temperature for a more reliable deep convective/cirrus clouds discrimination (Tjemkes et al. 1997). It is applied also in extratropical regions and is used for the identification of rain areas since these regions approximately represent the performance of many present optical rainfall retrievals.

The results were calculated at scale of pixel of SEVIRI images, in collocation with radar data. Each observation gives about 6,500 pair of pixels in co-coincidences. The evaluation parameters are determined from Table 1, in which a, b, c and d were values from a contingency table (Table 1). These parameters are calculated by using equations (7), (8), (9), (10), (11) and (12).

- The probability of detection (POD) measures the fraction of observed events that were correctly identified:

$$\mathrm{POD} = \frac{a}{a+c} \tag{7}$$

The optimal value of the POD is 1.

- The probability of false detection (POFD) indicates the fraction of pixels incorrectly identified by the satellite method.

$$\mathrm{POFD} = \frac{b}{b+d} \tag{8}$$

The optimal value of POFD is 0.

- The false alarm ratio (FAR) measures the fraction of estimated events that were actually not events:

$$\mathrm{FAR} = \frac{b}{a+b} \tag{9}$$

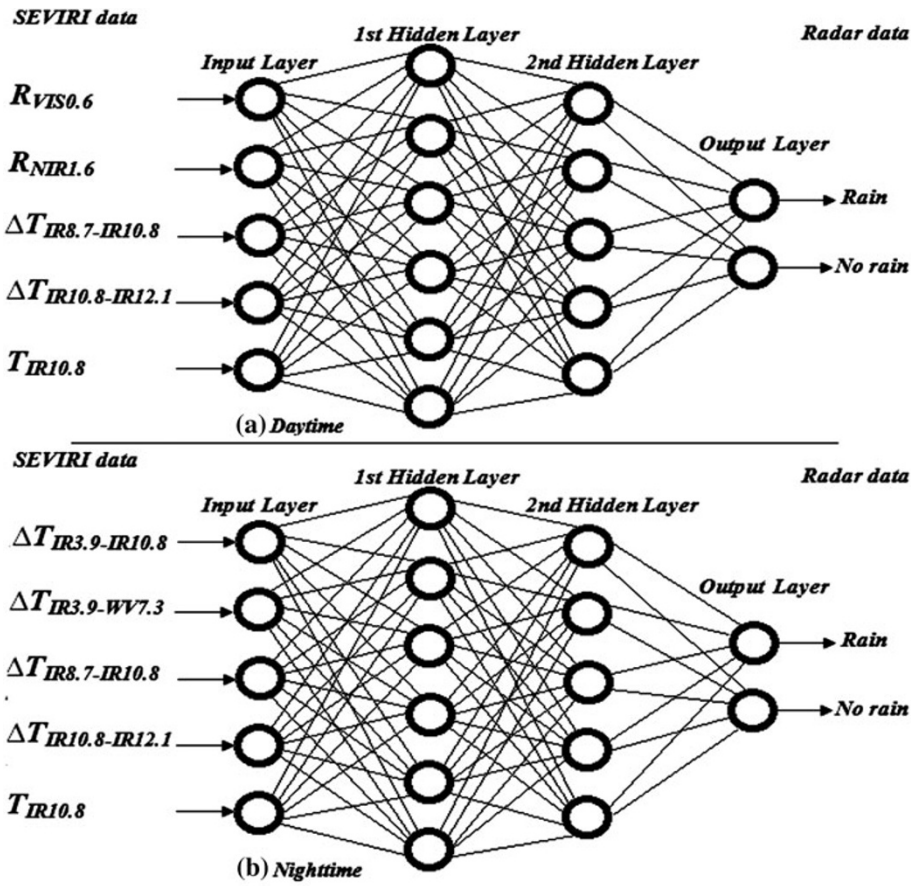

Fig. 5 Structure of multilayer perceptron rain area delineation algorithm (MLP) that combines spectral parameters from SEVIRI satellite images **a** during daytime and **b** during nighttime

Table 1 Overview of the combinations in a contingency table

Identified by satellite method	Observed by radar		
	Raining	No raining	Total
Raining	a	b	$a + b$
No raining	c	d	$c + d$
Total	$a + c$	$b + d$	$a + b + c + d = n$

Its optimal value is 0.

- The frequency BIAS index (Bias):

$$\text{Bias} = \frac{a+b}{a+c} \tag{10}$$

The optimal value of the Bias is 1. It measures the overestimation or underestimation of the method. A Bias greater than 1 indicates an overestimation, while a Bias lower than 1 indicates an underestimation.

- The Critical Success Index (CSI) measures the fraction of observed and/or estimated events that were correctly diagnosed:

$$\text{CSI} = \frac{a}{a+b+c} \tag{11}$$

The optimal value of CSI is 1.

- The percentage of corrects (PC) is the percentage of correct estimations:

$$\text{PC} = \frac{a+d}{n} \tag{12}$$

The optimal value of PC is 1.

The statistical results of the verification for MLP and ECST are given in the following table:

The area percentage of raining cloud classified by the proposed algorithm is almost consistent with those detected by the ground-based radar during daytime (Table 2). The good POD value is accompanied by a very low POFD value and the relatively low FAR. The values are 0.78, 0.03 and 0.21, respectively. The CSI indicates a good degree of correctly classified pixels. Bias parameter shows that the technique slightly underestimates the precipitation. It indicates a value of 0.69. The accuracy score shows that large fractions (PC 98 %) of the pixels are correctly identified as rainy or non-rainy by MLP. However, it is

Table 2 Results of evaluation parameters

	POD	POFD	FAR	Bias	CSI	PC
Day						
ECST	0.65	0.06	0.29	0.85	0.57	0.94
MLP	0.78	0.03	0.21	0.95	0.69	0.98
Night						
ECST	0.62	0.05	0.30	0.85	0.58	0.92
MLP	0.73	0.04	0.26	0.94	0.66	0.96
Total						
ECST	0.64	0.06	0.29	0.85	0.58	0.93
MLP	0.77	0.04	0.24	0.94	0.68	0.97
Optimal values	1	0	0	1	1	1

recognized that this result is heavily influenced by the high occurrence of non-rainy pixels. All these results indicate that the best values are obtained for MLP compared to ECST (Table 2).

The results obtained during nighttime are almost similar to those obtained during daytime. Indeed, the area fraction of raining cloud classified by the satellite-based technique is in good agreement with the corresponding area detected by the radar. The POD indicates that on average about 73 % of the pixels classified as raining cloud by the radar are consistently identified by the proposed scheme and it is more important than ECST technique. Compared to ECST technique, the FAR and the POFD are also lower and so indicate good performance. The high CSI value further supports the overall good performance of the technique with a better value. The slight underestimation by the ECST is a bit more pronounced than MLP.

For the total scenes, the identified fraction of raining cloud reveals a positive performance of the new differentiation scheme. The better performance of the daytime scheme for identifying precipitation area is probably due to the higher information content about the CWP inherent in the VIS0.6 and NIR1.6 channel compared to the four channel differences considered in the nighttime scheme.

The accuracy score shows that large fractions (97 %) of the pixels are correctly identified as rainy or non-rainy by MLP. The Bias score (0.95 for MLP and 0.85 for ECST) indicates that both MLP and ECST have a general tendency to underestimate rainy pixels. POD shows that 77 % of the rainy area is correctly detected by MLP, while ECST detects 64 % of the rainy area correctly. FAR reports that 24 and 29 % of the pixels detected as rainy by MLP and ECST, respectively, are false alarms.

To gain a visual impression of the performance of the introduced retrieval scheme, the classified rain area for a scene from Mars 09, 2011 (12:30 UTC) is depicted in Fig. 6. Figure 6a shows the brightness temperature in the channel IR10.8. Figure 6b shows the rain area classified by

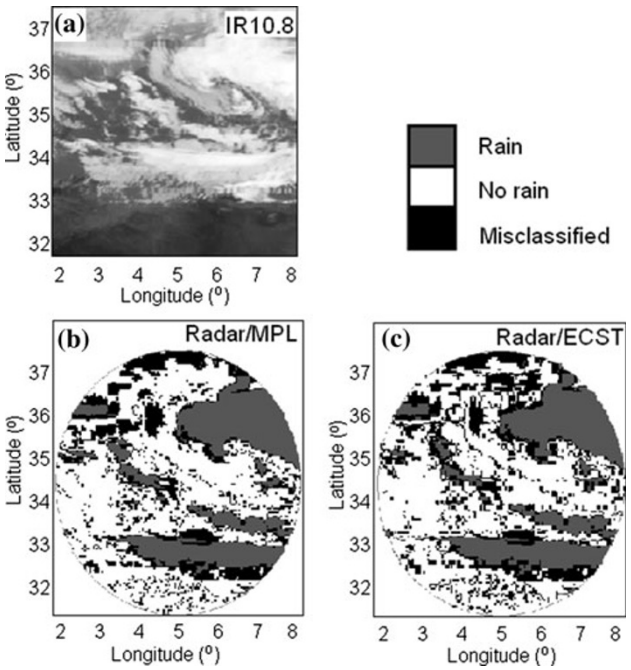

Fig. 6 Delineated rain area for the scene from Mars 09, 2011 (12:30 UTC). **a** BT10.8 image, **b** rain area delineated by Radar and MLP **c** rain area detected by Radar and ECST

both the new developed scheme and the radar. Figure 6c shows the rain area classified by both the ECST and radar.

The number of misclassified pixels is more important for the ECST method than for the MLP method. This visual results support the statistics results obtained previously. It should be noted that for scenes classified by the ECST, the results show that the identification of raining clouds still unsatisfactory in the mid-latitudes.

To summarize the results of the comparison study, an overall good performance of the proposed scheme can be stated, especially concerning the high temporal resolution of 15 min and the high spatial resolution of 3 × 3 km in sub-satellite (4 × 5 km in study area). Thus, a process-oriented separation of areas according to the conceptual model introduced in this study is possible.

Conclusion

A new consistent day and night technique for precipitation process separation and rainfall intensity differentiation using MSG SEVIRI data is proposed. It relies on information about the CWP, the CP in the upper regions, and the cloud top height (CTH). This technique is based on the new conceptual model that precipitation is favored by a large CWP and the presence of ice particles in the upper part of the cloud. The technique considers information about both parameters inherent in the channel differences $\Delta T_{\mathrm{IR3.9–IR10.8}}$, $\Delta T_{\mathrm{IR3.9–IR7.3}}$, $\Delta T_{\mathrm{IR8.7–IR10.8}}$, $\Delta T_{\mathrm{IR10.8–IR12.1}}$

and brightness temperature $T_{IR10.8}$, to detect potentially precipitating cloud areas during nighttime and reflectances $R_{VIS0.6}$, $R_{NIR1.6}$, brightness temperature $T_{IR10.8}$, brightness temperature difference $\Delta T_{IR8.7–IR10.8}$ and $\Delta T_{IR10.8–IR12.0}$ during the daytime. All parameters are used to gain implicit knowledge about the CWP and the cloud phase.

Together nighttime and daytime, the new algorithm offers the great potential for a 24-h technique for rain area delineation with a high spatial and temporal resolution.

The present study has demonstrated the great potential offered by the increased spectral resolution of MSG/SEVIRI. The spectral parameters are adjusted to geoclimatic conditions of the Mediterranean region. Indeed, the incorporation of multispectral information about optical and microphysical cloud properties has improved the identification of precipitating clouds. The results of identification by the MLP method were compared with radar data. The proposed technique is more efficient than existing techniques based only on information about the cloud-top temperature. The algorithm shows encouraging performance for the delineation of raining area in middle latitudes.

A further improvement in the identification performance of a neural network algorithm can be investigated if a wider set of input/output patterns, which are representative of different meteorological and geographical situations, is provided to the network during the training phase. Another possible way to optimize the estimate capability of a NN-based system is to use multisensory information at a higher sampling rate, using the MSG data from different multispectral channels.

References

Adler RF, Negri AJ (1988) A satellite infrared technique to estimate tropical convective and stratiform rainfall. J Appl Meteorol 27:30–51

Alpert P, Baldi M, Ilani R, Krichak S, Price C, Rodo′ X, Saaroni H, Ziv B, Kishcha P, Barkan J, Mariotti A, Xoplaki E (2006) Relations between climate variability in the Mediterranean region and the tropics: ENSO, South Asian and African monsoons, hurricanes and Saharan dust. In: Mediterranean climate variability. Elsevier, Amsterdam, pp 149–177

Arkin PA (1979) The relationship between the fractional coverage of high cloud and rainfall accumulations during GATE over the Bscale array. Mon Weather Rev 107:1382–1387

Arking A, Childs JD (1985) Retrieval of cloud cover parameters from multispectral satellite images. J Appl Meteorol 24:322–333

Baum BA, Soulen PF, Strabala KI, King MD, Ackerman SA, Menzel WP, Yang P (2000) Remote sensing of cloud properties using MODIS airborne simulator imagery during SUCCESS. J Geophys Res 105:11,781–11,792

Bellerby T, Todd M, Kniveton D, Kidd C (2000) Rainfall estimation from a combination of TRMM precipitation radar and GOES multispectral satellite imagery through the use of an artificial neural network. J Appl Meteorol 39:2115–2128

Bendix J (1997) Adjustment of the Convective-Stratiform Technique (CST) to estimate 1991/93 El Ninorainfall distribution in Ecuador and Peru by means of Meteosat-3 IR data. Int J Remote Sens 18:1387–1394 and 2707

Berges JC, Jobard I, Chopin F, Roca R (2010) EPSAT-SG: a satellite method for precipitation estimation; its concepts and implementation for the AMMA experiment. Ann Geophys 28:289–308

Ebert EE, Manton MJ, Arkin PA, Allam RJ, Holpin GE, Gruber A (1996) Results from the GPCP algorithm intercomparison projects. Bull Am Meteorol Soc 77:2875–2887

EUMETSAT (2004) Applications of Meteosat Second Generation—conversion from counts to radiances and from radiances to brightness temperatures and reflectance. http://oiswww.eumetsat.org/WEBOPS/msg_interpretation/index.html

Feidas H (2011) Study of a mesoscale convective complex over the eastern Mediterranean basin with Meteosat data. In: 2011 Eumetsat Meteorological Satellite Conference, Oslo, Norway, 5–9 September, 2011

Feidas H, Giannakos A (2010) Identifying precipitating clouds in Greece using multispectral infrared Meteosat Second Generation satellite data. Theor Appl Climatol. doi:10.1007/s00704-010-0316-5

Feidas H, Giannakos A (2011) Classifying convective and stratiform rain using multispectral infrared Meteosat Second Generation satellite data. Theor Appl Climatol. doi:10.1007/s00704-011-0557-y

Grimes DIF, Pardo E, Bonifacio R (1999) Optimal areal rainfall estimation using raingauges and satellite data. J Hydrol 222:93–108

Grimes DIF, Coppola E, Verdecchia M, Visconti G (2003) A neural network approach to real-time rainfall estimation for Africa using satellite data. J Hydrometeorol 4:1119–1133

Haykin S (1994) Neural networks. Macmillan, New York

Herman A, Kumar V, Arkin P, Kousky J (1997) Objectively determined 10-day African rainfall estimates created for famine early warning systems. Int J Rem Sens 18(10):2147–2159

Houze Jr (1993) Cloud dynamics. Academic Press, San Diego

Huffman GJ, Adler RF, Morrissey MM, Bolvin DT, Curtis S, Joyce R, McGavock B, Susskind J (2001) Global precipitation at one-degree daily resolution from multisatellite observations. J Hydrometeorol 2:36–50. doi:10.1175/1525-7541(2001)002<0036:GPAODD>2.0.CO;2

Hutchison K, Wong E, Ou SC (2006) Cloud base heights retrieved during night-time conditions with MODIS data. Int J Remote Sens 27:2847–2862

Inoue T (1985) On the temperature and effective emissivity determination of semi-transparent cirrus clouds by bi-spectral measurements in the 10-mm window region. J Meteorol Soc Jpn 63:88–99

Inoue T (1987a) A cloud type classification with NOAA-7 splitwindow measurements. J Geophys Res 92:3991–4000

Inoue T (1987b) An instantaneous delineation of convective rainfall areas using split window data of NOAA-7 AVHRR. J Meteorol Soc Jpn 65:469–481

Inoue T (1997) Day-to-night cloudiness change of cloud types inferred from split window measurements aboard NOAA polarorbiting satellites. J Meteorol Soc Jpn 75:59–66

Inoue T, Wu X, Bessho K (2001) Life cycle of convective activity in terms of cloud type observed by split window. In: 11th Conference on Satellite Meteorology and Oceanography, Madison, WI, USA

Jobard I, Chopin F, Berges JC, Roca R (2011) An intercomparison of 10-day satellite precipitation products during West African

monsoon. Int J Rem Sens 32(9):2353–2376. doi:10.1080/01431161003698286
Kobayashi T (2007) Significant differences in the cloud droplet effective radius bet nonprecipitating and precipitating clouds. Geophys Res Lett 34:L15811. doi:10.1029/2007GL029606
Lensky IM, Rosenfeld D (2003a) A night-rain delineation algorithm for infrared satellite data based on microphysical considerations. J Appl Meteorol 42:1218–1226
Lensky IM, Rosenfeld D (2003b) Satellite-based insights into precipitation formation processes in continental and maritime convective clouds at nighttime. J Appl Meteorol 42:1227–1233
Levizzani V (2003) Satellite rainfall estimations: new perspectives for meteorology and climate from the EURAINSAT project. Ann Geophys 46:363–372
Levizzani V, Schmetz J, Lutz HJ, Kerkmann J, Alberoni PP, Cervino M (2001) Precipitation estimations from geostationary orbit and prospects for Meteosat Second Generation. Meteorol Appl 8:23–41
Lionello P, Malanotte-Rizzoli P, Boscolo R, Alpert P, Artale V, Li L, Luterbacher J, May W, Trigo R, Tsimplis M, Ulbrich U, Xoplaki E (2006) The Mediterranean climate: an overview of the main characteristics and issues. In: Mediterranean climate variability. Elsevier, Amsterdam, pp 1–26
Mishra AK, Gairola RM, Varma AK, Vijay KA (2011) Improved rainfall estimation over the Indian region using satellite infrared technique. Adv Space Res. doi:10.1016/j.asr.2011.02.016
Nauss T, Kokhanovsky AA (2006) Discriminating raining from non-raining clouds at mid latitudes using multispectral satellite data. Atmos Chem Phys 6:5031–5036
Negri AJ, Adler RF (1993) An intercomparison of three satellite infrared rainfall techniques over Japan and surrounding waters. J Appl Meteorol 32:357–373
Platnick S, King MD, Ackerman SA, Menzel WP, Baum BA, Riedi JC, Frey RA (2003) The MODIS cloud products: algorithms and examples from Terra. IEEE Trans Geosci Remote Sens 41:459–473
Reudenbach C, Heinemann G, Heuel E, Bendix J, Winiger M (2001) Investigation of summertime convective rainfall in Western Europe based on a synergy of remote sensing data and numerical models. Meteorol Atmos Phys 76:23–41
Roebeling RA, Holleman I (2009) Validation of rain rate retrievals from SEVIRI using weather radar observations. J Geophys Res 114:D21202. doi:10.1029/2009JD012102
Roebeling RA, Deneke HM, Feijt AJ (2007) Validation of cloud liquid water path retrievals from SEVIRI using one year of CloudNET observations. J Appl Meteorol Climatol 47:206–222
Rosenblatt F (1962) Principles of neurodynamics: perceptrons and the theory of brain mechanisms. Spartan Books, Washington, DC
Rossow WB, Schiffer RA (1999) Advances in understanding clouds from ISCCP. Bull Am Meteorol Soc 80:2261–2287
Schmetz J, Pili P, Tjemkes S, Just D, Kerkmann J, Rota S, Ratier A (2002). An introduction to Meteosat Second Generation (MSG). Bull Amer Meteorol Soc 83:977–992. http://dx.doi.org/10.1175/1520-0477(2002)083<0977:AITMSG>2.3.CO;2
Stephens GL, Kummerow CD (2007) The remote sensing of clouds and precipitation from space: a review. J Atmos Sci Special Sect 64:3742–3765
Strabala KI, Ackerman SA, Menzel WP (1994) Cloud properties inferred from 8–12-μm data. J Appl Meteorol 33:212–229
Tapiador FJ, Kidd C, Levizzani V, Marzano FS (2004) A neural networks-based fusion technique to estimate halfhourly rainfall estimates at 0.18 resolution from satellite passive microwave and infrared data. J Appl Meteorol 43:576–594
Tarruella R, Jorge J (2003) Comparison of three infrared satellite techniques to estimate accumulated rainfall over the Iberian Peninsula. Int J Climatol 23:1757–1769
Thies B, Nauss T, Bendix J (2008a) Discriminating raining from non-raining clouds at mid-latitudes using meteosat second generation daytime data. Atmos Chem Phys 8:2341–2349
Thies B, Nauss T, Bendix J (2008b) Delineation of raining from non-raining clouds during nighttime using Meteosat-8 data. Meteorol Appl 15:219–230
Tjemkes SA, Van de berg L, Schmetz J (1997) Warm water vapour pixels over high clouds as observed by Meteosat. Contrib Atmos Phys 70:15–21
Trigo RM, Xoplaki E, Lüterbacher J, Krichak SO, Alpert P, Jacobeit J, Sáenz J, Fernández J, González-Rouco JF (2006) Relations between variability in the Mediterranean region and mid-latitude variability. In: Lionello P, Malanotte-Rizzoli P, Boscolo R (eds) Mediterranean climate variability. Elsevier, Amsterdam, pp 179–226
Vicente GA, Davenport JC, Scofield RA (2002) The role of orographic and parallax corrections on real time high resolution satellite rainfall rate distribution. Int J Remote Sens 23(2):221–230
Wentz FJ, Spencer RW (1998) SSM/I rain retrievals within a unified all-weather ocean algorithm. J Atmos Sci 55:1613–1627
Wolters ELA, Roebeling RA, Feijt AJ (2008) Evaluation of cloud phase retrieval methods for SEVIRI onboard Meteosat-8 using ground-based lidar and cloud radar data. J Appl Meteorol Climatol 47:1723–1738. doi:10.1175/2007JAMC1591.1
Wolters ELA, Van Den Hurk BJJM, Roebeling RA (2011) Evaluation of rainfall retrievals from SEVIRI reflectances over West Africa using TRMM-PR and CMORPH. Hydrol Earth Syst Sci 15:437–451